AEROSPACE REPORT NO.
TR-2006(8565)-3

Measurements and Modeling of $SiCl_4$ Combustion in a Low-Pressure H_2/O_2 Flame

10 November 2006

Prepared by

T. MOORE, B. BRADY, and L. R. MARTIN
Space Materials Laboratory
Laboratory Operations

Prepared for

SPACE AND MISSILE SYSTEMS CENTER
AIR FORCE SPACE COMMAND
483 N. Aviation Blvd.
El Segundo, CA 90245-2808

Engineering and Technology Group

THE AEROSPACE CORPORATION
El Segundo, California

This report was submitted by The Aerospace Corporation, El Segundo, CA 90245-4691, under Contract No. FA8802-04-C-0001 with the Space and Missile Systems Center, 483 N. Aviation Blvd., El Segundo, CA 90245. It was reviewed and approved for The Aerospace Corporation by G. F. Hawkins, Principal Director, Space Materials Laboratory; and D. C. Marvin, Principal Director, Office of Research & Technology Applications. Michael Zambrana was the project officer for the Mission-Oriented Investigation and Experimentation (MOIE) program.

This report has been reviewed by the Public Affairs Office (PAS) and is releasable to the National Technical Information Service (NTIS). At NTIS, it will be available to the general public, including foreign nationals.

This technical report has been reviewed and is approved for publication. Publication of this report does not constitute Air Force approval of the report's findings or conclusions. It is published only for the exchange and stimulation of ideas.

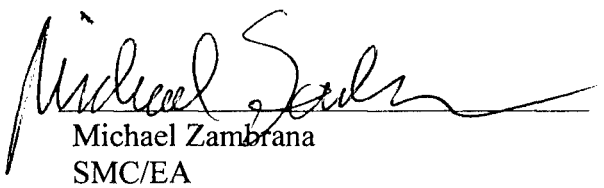

Michael Zambrana
SMC/EA

REPORT DOCUMENTATION PAGE

Form Approved
OMB No. 0704-0188

1. REPORT DATE (*DD-MM-YYYY*)	2. REPORT TYPE	3. DATES COVERED (*From - To*)
10-09-2006		

4. TITLE AND SUBTITLE

Measurements and Modeling of $SiCl_4$ Combustion in a Low-Pressure H_2/O_2 Flame

5a. CONTRACT NUMBER
FA8802-04-C-0001

5b. GRANT NUMBER

5c. PROGRAM ELEMENT NUMBER

6. AUTHOR(S)

T. Moore, B. Brady, and L. R. Martin

5d. PROJECT NUMBER

5e. TASK NUMBER

5f. WORK UNIT NUMBER

7. PERFORMING ORGANIZATION NAME(S) AND ADDRESS(ES)

The Aerospace Corporation
Laboratory Operations
El Segundo, CA 90245-4691

8. PERFORMING ORGANIZATION REPORT NUMBER

TR-2006(8565)-3

9. SPONSORING / MONITORING AGENCY NAME(S) AND ADDRESS(ES)

Space and Missile Systems Center
Air Force Space Command
483 N. Aviation Blvd.
El Segundo, CA 90245

10. SPONSOR/MONITOR'S ACRONYM(S)
SMC

11. SPONSOR/MONITOR'S REPORT NUMBER(S)

12. DISTRIBUTION/AVAILABILITY STATEMENT

Approved for public release; distribution unlimited.

13. SUPPLEMENTARY NOTES

14. ABSTRACT

Laser-Induced Fluorescence (LIF) was used to measure temperature and OH concentration profiles as a function of distance from a McKenna-style burner in premixed, one-dimensional, low-pressure H_2/O_2/Ar $SiCl_4$-doped flames. The addition of $SiCl_4$ was shown to affect the flame temperature and OH concentration profiles. A gas-phase chemical kinetics mechanism for the combustion of $SiCl_4$ in an H_2/O_2/Ar flame was proposed, and experimental results were compared with predictions for a premixed, one-dimensional laminar flame model based on CHEMKIN. The low-pressure flame data are sensitive to the overall kinetics of the mechanism. In order to obtain the best fit to the observed data for all flame configurations, we had to modify six different rates from our original estimates. None of the modified rates are well known for the temperature regime of our flame. Particle formation and surface chemistry were not taken into account.

15. SUBJECT TERMS

Low-pressure flame, SiCl4, Silicon tetrachloride, Combustion synthesis, Flame synthesis, Kinetics mechanism

16. SECURITY CLASSIFICATION OF:			17. LIMITATION OF ABSTRACT	18. NUMBER OF PAGES	19a. NAME OF RESPONSIBLE PERSON
					Teresa Moore
a. REPORT	b. ABSTRACT	c. THIS PAGE			19b. TELEPHONE NUMBER (*include area code*)
UNCLASSIFIED	UNCLASSIFIED	UNCLASSIFIED		24	(310)336-2486

Contents

Figures

Tables

1. Introduction

Formation of high-purity powders and glasses via flame aerosol processes is important for many industries, including fiber optics, ceramics, and semiconductors. Although many studies[1,2] have been carried out on the formation of silicon dioxide (SiO_2) by burning various silicon-containing precursors, the fundamental chemical kinetics leading to particle formation are not well understood. Modeling the gas-phase chemical kinetics is difficult due to the paucity of fundamental data,[1] including the primary reaction pathways and the intermediate species. Silane combustion has been the most studied; several detailed chemical kinetics mechanisms for silane combustion varying in complexity and physical processes considered have been proposed.[3,4,5] Combustion of other silicon precursors is less well understood.

Many of the experimental and modeling efforts on the formation of SiO_2 in a flame have focused on determining final particle size and morphology. For recent reviews on the formation of oxides in flames, see Wooldridge[1] and Pratsinis.[2] The physical flame configuration and temperature profile[6] determine the extent to which precursor identity and kinetics affect the final particle size, morphology, and composition. Several studies have shown that addition of a silicon-containing dopant to diffusion and premixed flames can significantly affect flame characteristics, including temperature and species concentrations.[7,8,9,10] Because temperature[6] is an important influence on the final particle characteristics and the kinetics affect the flame temperature, understanding chemical kinetics of the flame is important for understanding and predicting final particle characteristics.

There are several models that deal with particle formation, but to date, no detailed chemical kinetics mechanisms for the reaction of silicon tetrachloride ($SiCl_4$) in hydrogen/oxygen flames have been published. A simple chemical kinetics mechanism based on an initial reaction of $SiCl_4 + H_2O$ was proposed by Hannebauer and Menzel.[11] $SiCl_4$ combustion is often modeled by simplifying the kinetics to the overall oxidation ($SiCl_4 + O_2 \rightarrow SiO_2 + 2\ Cl_2$) or hydrolysis ($SiCl_4 + H_2O \rightarrow SiO_2 + 4HCl$) reactions,[2] or by using several rate-determining steps[12] to model the flame chemistry.

Various less complex systems involving $SiCl_4 + O_2$ or $SiCl_4 + H_2$ reactions for lower-temperature chemical vapor deposition applications have been modeled,[13,14,15] but for the most part, these models either include a very simplified kinetics scheme[16,17] or dismiss kinetics all together.[18] One model[19,20,21,22] proposed a low-temperature $SiCl_4 + O_2$ mechanism in which large chlorosiloxane chains and cyclic compounds are formed, progressively becoming more and more like SiO_2 with time. However, none of these models represents the conditions in a flame environment.

While these approaches to modeling can yield valuable information, a more detailed model of the flame chemical kinetics is necessary to fully understand the initial particle formation process and how it relates to the final particle properties. We have proposed a gas-phase chemical kinetics mechanism for the combustion of $SiCl_4$ in an $H_2/O_2/Ar$ flame. In this report, we report measurements of temperature and OH concentration profiles for a premixed, one-dimensional, low-pressure flat $H_2/O_2/Ar$ flame doped with $SiCl_4$. We compare these data to modeling results using our mechanism and the

CHEMKIN modeling software.[23],[24] The goal of this experiment was to test the overall reaction kinetics of our model in a one-dimensional, premixed flat flame where the role of fluid mechanics was simplified.

Heterogeneous chemistry and particle formation were not included in the model. This is not because these processes are negligible or unimportant, but because there is no good treatment for modeling their impact on a low-pressure flame. There are good modeling treatments for these processes,[25,26,27] including the CHEMKIN package, but models that include heterogeneous processes do not include the transport mechanisms that are important in this flame. We chose the current model because it is the standard tool for modeling low-pressure flames.

We used a low-pressure flame technique[28] because the homogeneous flame reaction zone and the particle formation region is significantly elongated compared to atmospheric-pressure flames. This increases the spatial resolution with which we can probe the temperature and species concentrations. Our main diagnostic technique for measuring radical species concentrations was Laser-Induced Fluorescence (LIF).[29]

2. Experiment

Figure 1 shows a diagram of our low-pressure flame apparatus. A low-pressure porous plug flat-flame burner was mounted on a three-axis translator in a vertical flow configuration. The chamber pressure was maintained at 30±0.5 Torr; it was servo-controlled by using a 100 Torr capacitance manometer to provide feedback to a throttle valve on the vacuum pump line. The mechanical pump on the chamber was purged with nitrogen and equipped with mechanical traps to capture particles.

The combustion gases were mixed in a small manifold before entering the burner. The gas flows were regulated by computer-controlled mass flow controllers. The burner outer shield flow was run at 2.7 standard liters per minute (SLM) of argon to help keep the premixed combustion zone one-dimensional. The total flow rate through the burner was kept constant at 2.25 SLM.

Three basic flame configurations were studied: an undiluted stoichiometric H_2/O_2 flame, a diluted stoichiometric H_2/O_2 flame with 35% of the total flow as argon diluent, and a fuel-rich undiluted flame with $\Phi = 1.2$. These flames were studied with and without $SiCl_4$ precursor at concentrations of 0.5% of the $H_2 + O_2$ flow. For the experiments doped with $SiCl_4$, the oxygen flow exiting the flow meter was bubbled through a Teflon-coated stainless-steel cell containing $SiCl_4$ before being mixed with the other gases. The cell was temperature controlled to within ±0.005 °C. $SiCl_4$ concentration was determined from the vapor pressure and total pressure measurements, which were carried out with capacitance manometers. The $SiCl_4$ cell was weighed before and after each experiment and compared to the calculated mass loss to confirm the calculated $SiCl_4$ flow rates.

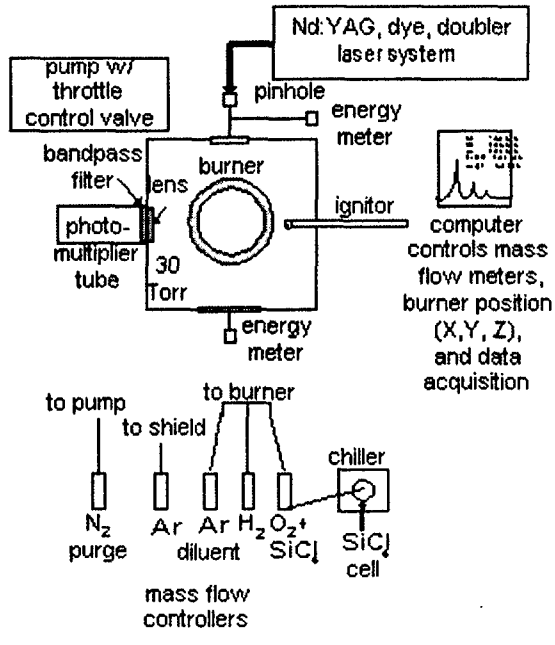

Figure 1. Schematic of low-pressure flame apparatus.

Temperature and OH concentration profiles were obtained using a standard laser-induced fluorescence (LIF) technique modified for use in a particle-forming combustion environment.[9] The laser system consisted of a dye laser pumped by a Nd:YAG laser operating at 532 nm and 30 Hz. The resulting output was doubled with a KDP crystal and then irised to ~0.6 mm diameter before being sent into the vacuum chamber. The fluorescence was collected perpendicular to the laser axis with a lens filtered by 308±15-nm bandpass filters and then focused onto a photomultiplier tube. Signals were processed by a boxcar integrator triggered by the Nd:YAG laser. A short (15 ns) gate coincident with the laser pulse was used in order to reduce quenching effects on the signal. Power meters recorded the power both before and after the chamber, allowing the fluorescence signal to be corrected for fluctuations in laser intensity. Typical laser energy used was 0.3–2.0 μJ/pulse. Experiments were performed to verify that these energies were low enough to avoid saturation of the OH transition. The optics were purged with argon to avoid particle deposition.

For temperature and OH concentration measurements, select transitions in the (1←0) band of the $A \leftarrow X$ system were excited and the broadband fluorescence around 310 nm was observed. For temperature measurements, the relative intensities of the $P_1(2)$ and $R_1(14)$ lines near 282.6 nm were used.[30] The error in the temperature determined by utilizing these two lines is small, less than 5% for the entire range from 500K to 2500K.[31] Temperatures were derived by comparing the relative integrated intensity of these two lines in the experimental spectra to those in spectra predicted at various temperatures using the computer program LIFBASE.[32] The pressure was put into the LIFBASE program and Doppler, predissociation, and collisional broadening were included in the spectral simulations. The instrument resolution parameter was adjusted until the predicted peak width matched our observed data, which occurred at an instrument resolution of 0.035Å. Then a series of simulated spectra were run for temperatures over the expected experimental temperature range of 500–2000K. A relation for temperature as a function of the ratio of the areas under the $P_1(2)$ and $R_1(14)$ peaks was obtained. This function was then used to generate a temperature for each experimental spectrum by using the integrated intensities of the observed $P_1(2)$ and $R_1(14)$ peaks after correcting for laser power. The relative OH concentration was measured by comparing the integrated intensity of each of these lines after correcting for the temperature dependence. This method gave OH concentration profiles similar to those obtained by monitoring the $P_1(8)$ line at 285.66 nm, which has been shown to be relatively insensitive to temperature from 1200K to 2500K.[9]

In these experiments, we measured relative OH concentrations. Absolute concentrations were not measured due to the complexity of accounting for excited-state quenching. In order to obtain an absolute concentration without making a quantitative absorption measurement for calibration, the identity, concentration, and quenching cross section of each species that might collide with the OH must be known at every point. In the flames with no diluent, the main quenching species is water, but in the flames with argon diluent, the argon also plays an important role in quenching. Argon has a quenching cross section for OH that is several orders of magnitude smaller than that of water.[33] Because the quenching environment is so different in the experiments with and without diluent, the relative OH signals for experiments with diluent cannot be directly compared to those in experiments without diluent. The addition of argon increased the width of the time evolution of the OH fluorescence signal, especially in the tail. Based on the changes in the width and shape of this signal as argon was added, it seems to be very sensitive to the quenching rate. The addition of small amounts of $SiCl_4$ did not perturb the width or shape of the time evolution of the OH fluorescence signal. Thus, we assume that the change in the quenching environment on addition of small amounts of $SiCl_4$ is

sufficiently small that we can compare OH concentrations for experiments with the same basic flame configuration with and without $SiCl_4$ precursor.

Hydroxyl concentration and temperature were monitored as a function of distance from the burner. A burner position of "0.0 cm" indicates that the burner blocks half of the 0.6-mm-dia laser beam. The burner was moved through several centimeters for each data run, with data being collected at various distances from the burner. Although we collected data out to 6 cm from the burner for some runs, most runs ended at 3 cm, at which point combustion is substantially complete. Beyond 3 cm from the burner, the temperature and OH concentration depend mostly on the rate of heat loss from the apparatus, which does not shed any light on the chemistry. The error bars shown in the figures represent one standard deviation based on several data runs.

3. Mechanism and Model

Table 1 outlines our proposed combustion mechanism for $SiCl_4$ in a hydrogen/oxygen flame. Rates for the first thermal decomposition step and the first hydrogen abstraction step were available in

Table 1. Silicon Tetrachloride Proposed Combustion Mechanism ($k = AT^b e^{-E/RT}$). The units of A are cc/molecule-s for second-order reactions; higher order reactions have higher power inverse concentration units. The activation energy E is in kJ/mol.

Reaction	A	b	E	Source
$SiCl_4 + M = SiCl_3 + Cl + M$	4.8e16	0	392	Experiment[34]
$SiCl_4 + H = SiCl_3 + HCl$	**1.7e13**	**0**	**29**	**This work**
Original rate:	1.4e13	0	40	Experiment[35]
$SiCl_3 + O_2 + M = SiCl_3O_2 + M$	8.7e12	0	0	Experiment[36]
$SiCl_3O_2 + M = SiCl_3O + O + M$	1.0e13	0	59	Analogy[5]
$SiCl_3O + H = SiCl_2O + HCl$	1.6e17	-1.4	6	Analogy[42]
$SiCl_3O_2 + HO_2 = SiCl_3O_2H + O_2$	4.0e9	0	0	Analogy[5]
$SiCl_2O + M = SiO + Cl_2 + M$	1.0e12	0	254	Analogy[42]
$SiCl_2O + H = SiClO + HCl$	**2.0e14**	**0**	**21**	**This work**
Original rate:	3.3e13	0	44	Analogy[5]
$SiClO + M = SiO + Cl + M$	**1.0e14**	**0**	**33**	**This work**
Original rate:	5.4e13	0	121	Analogy[5]
$SiClO + H = SiO + HCl$	**3.0e15**	**0**	**0**	**This work**
Original rate:	2.0e13	0	0	Analogy[5]
$SiCl_3 + H = SiCl_2 + HCl$	1.5e12	0	10	Analogy[4]
$SiCl_2 + H = SiCl + HCl$	1.4e12	0	8	Analogy[42]
$SiCl_2 + O_2 = SiCl_2O + O$	3.4e12	0	0	Experiment[37]
$SiCl_2 + O = SiO + Cl_2$	4.6e12	0	0	Analogy[38]
$SiCl + O = SiO + Cl$	4.0e12	0	0	Analogy[42]
$SiCl_3O + H_2 = SiCl_3OH + H$	1.2e11	0	4	Analogy[5]
$SiCl_3O_2 + H_2 = SiCl_3O_2H + H$	1.3e10	0	36	Analogy[5]
$SiCl_3O_2H + M = SiCl_3O + OH + M$	6.5e13	0	204	Analogy[5]
$SiCl_3OH + OH = SiCl_3O + H_20$	4.0e11	0	6	Analogy[5]
$SiCl_2O + H_2O = SiClO_2H + HCl$	4.0e12	0	81	Calculated[11]
$SiClO_2H + M = SiO_2 + HCl + M$	3.7e13	0	205	Calculated[11]
$SiCl_2O + OH = SiClO_2H + Cl$	1.0e12	0	0	Analogy[5]
$SiCl_3 + SiCl_3 = SiCl_2 + SiCl_4$	1.0e12	0	0	Fit[39]
$SiCl_3 + M = SiCl_2 + Cl + M$	1.0e14	0	272	Fit[39]
$SiCl_4 + H_2O = SiCl_3OH + HCl$	1.0e12	0	121	Experiment[40]
$SiCl_3OH + M = SiCl_2O + HCl + M$	2.8e13	0	207	Calculated[11]
$SiCl_4 + OH = SiCl_3OH + Cl$	1.4e7	0	188	Calculated[11]
$SiO + O_2 = SiO_2 + O$	**1.5e12**	**0**	**21**	**This work**

Reaction	A	b	E	Source
Original rate:	1.0e13	0	27	Estimated[41]
$SiO + OH = SiO_2 + H$	**3.0e10**	**0.8**	**0**	**This work**
Original rate:	1.8e10	0.78	5	Calculated[3]
$SiO + O + M = SiO_2 + M$	2.5e15	0	18	Analogy with CO[41]
$HCl + M = H + Cl + M$	4.4e13	0	342.1	NIST database[43]
$Cl^2 + M = 2Cl + M$	2.32e13	0	196.5	NIST database[43]
$H + Cl_2 = HCl + Cl$	1.91e13	0	0	NIST database[43]
$O + HCl = OH + Cl$	6.03e12	1.7	27.4	NIST database[43]
$OH + HCl = H_2O + Cl$	1.11e7	0	-2.8	NIST database[43]

papers by Catoire *et al.*[34,35] and Powers,[14] respectively. These papers suggested that the initial steps produce the radical $SiCl_3$ rather than $SiCl_2$. Because the analogous radical SiH_3 is an important species in the Takahashi *et al.* mechanism[5] for silane oxidation, we used this mechanism as a model for our silicon tetrachloride oxidation mechanism. Additional reactions for species in the mechanism were added whenever experimental,[36,37,38,39,40] calculated, or estimated[41] rates were available. The reactions were chosen as analogues of the corresponding reactions for silane, with the exception that no chlorine oxides were included since these are not stable enough to exist at the flame temperatures of interest. Also, we did not include any species in which hydrogen re-substituted on the silicon since this is unfavorable energetically. Analogous rates were taken from the Takahashi list[5] or the Zachariah mechanism.[42] When estimating chlorine rates from analogous hydrogen rates, rates were estimated as roughly 10 times slower for abstraction, dissociation, and transfer reactions, and roughly the same for decomposition and reactions, which required more indirect analogies. These estimates are based on the few reactions where experimental rate determinations have been made for both the silane rate and the analogous silicon chloride rate. There is not enough information to justify a more precise estimate. Because this estimate is so crude, we tried adjusting it by a factor of 10 in either direction during the fitting process to try to get better agreement with the experiment. Adjusting the rates as a group did not change the fit, but changing some of the individual rates in this group was helpful. HCl and Cl_2 reactions were added as necessary from the NIST database.[43] The GRI 3.0 mechanism[44] was used for the H_2/O_2 reactions. Particle formation and chemistry on particle surfaces were not included in the model. Because particle formation is a 3-body process, it is expected to occur relatively late in the flame. Because of diffusion, however, particles are distributed throughout the flame, and there is some potential for reactions on the particle surfaces to influence flame chemistry.

In three-body reactions, the reaction is dependant on a non-reacting collider molecule, or "third body," to transfer energy to or from the reacting species. Because energy transfer and storage vary greatly for different chemical species, different third-body colliders have different efficiencies at promoting the reaction. The GRI mechanism accounts for the difference in efficiency of various third bodies; for instance, argon is usually 1–3 orders of magnitude less efficient than water as a third body. Based on this, we have also reduced the efficiency of argon as a third body in the silicon reactions by 2 orders of magnitude.

We compared our data to results from a chemical kinetics model using our proposed $SiCl_4$ combustion mechanism and CHEMKIN. We chose the premixed burner reactor in the CHEMKIN program to model our one-dimensional flame. This model uses the measured temperature profile as an input.

We did a fit to our temperature data and used this fit as the model input. For each set of basic flame configurations, we scaled the measured relative OH concentrations to the model prediction for the OH concentration of the H_2/O_2 flame with no precursor.

The CHEMKIN transport subroutine requires input parameters to calculate the diffusivity of the various species. We estimated these parameters for silicon tetrachloride combustion species based on the methods outlined in "The Properties of Gases and Liquids" by Reid, Prausnitz, and Sherwood.[45] Values for the dipole moments came from the CRC handbook[46] where available; calculated values from Gaussian[47] were used where no measured values were available. The transport properties are shown in Table 2.

Table 2. Transport Database for Species from $SiCl_4$ Combustion. () = estimated quantity

Species Name	Geometry#	ε/k	σ	μ
HSiO	1	500	3.69	(2)
SiOH	1	363	4.11	(1)
SiH_2O	2	500	3.71	(2)
SiO	1	3150	2.96	3.1
SiO_2	1	4300	3.51	0
H_3SiOO	2	380	4.54	(1.5)
H_2SiOO	2	380	4.51	(1.5)
OSiOH	1	435	4.28	(2)
H_2SiO	2	4400	1.80	4.6
H_3SiO	2	2600	2.17	(4)
H_3SiOH	2	400	4.05	(1.5)
H_2SiOH	2	480	3.77	(2)
H_3SiOOH	2	380	4.56	(1.5)
OSiHOH	2	350	4.61	(0)
H_3SiOO^*	2	380	4.54	(1.5)
SiOOH	2	350	4.59	(0)
SiH_4	2	190	4.21	0
HSiOH	1	363	4.14	(1)
HSiOOH	1	435	4.31	(2)
Si_2O_2	2	2360	4.43	(0)
Si_2H	2	236	4.49	(0.1)
H_3Si_2H	2	300	5.19	(0.1)
SiCl	1	366	4.01	1.03
$SiCl_2$	1	360	4.69	0.95
$SiCl_3$	2	350	5.22	0.74
$SiCl_4$	2	390	5.64	0
$SiCl_3O_2$	2	473	5.60	(1)
$SiCl_3O$	2	473	5.41	(1)
$SiCl_2O$	2	970	3.90	3.79
$SiCl_3O_2H$	2	473	5.62	(1)
$SiCl_3OH$	2	473	5.42	(1)
$SiClO_2H$	2	476	4.65	(1)
SiClO	1	556	4.15	(2)

#: Geometry index. 0 = monatomic, 1 = linear, 2 = nonlinear
ε/k, Lennard-Jones well depth in Kelvins
σ, Lennard-Jones collision diameter in Angstroms
μ, Dipole moment in Debye units.

The modeling work required additional thermodynamic data for the CHEMKIN database. The thermodynamic data are necessary to calculate the reverse rate of reactions. This database consists of sets of coefficients that represent the entropy, enthalpy, and heat capacity of each substance as a power series expansion in terms of temperature. The expansion used in CHEMKIN is the Gordon and McBride representation.[24] Most of the literature values, including the NIST database,[43] are given as Shomate coefficients, which are for a similar, but not identical, expansion. We were able to relate the two sets of coefficients by approximation. Enthalpies as a function of temperature calculated from the converted coefficients were compared with the JANAF Tables[48] where possible. This approach was found to give results consistent to about 1% for molecules in the NIST database. For species not in the NIST database, the estimated thermodynamic quantities were taken from formal calculations, such as those in Zachariah and Tsang[3] or Allendorf, *et al.*[49] For species not in the NIST database and for which no formal calculations exist, we use the three-term representation:

$$a_1 = C_p/R$$

$$a_6 = H^\circ/R - a_1(298)$$

$$a_7 = S^\circ/R - a_1 \ln(298)$$

In addition, we used approximations for the heat capacity and the entropy terms for molecules where these are not available. For the heat capacity, we use the classical mechanics approximation: $C_p = (3n - 2)R$, where n is the number of atoms in the molecule. For the entropy, we use an empirical correlation with the molecular weight: $S^\circ = 167 + 2.163(\text{M.W.})$ J/mol/K. The enthalpy was based on approximate bond-additivity relations. The thermodynamic coefficients are listed in Table 3.

Table 3. Thermodynamic Data for the Silicon Species in Mechanism. Species with a5 = 0 are from NIST database. Species with all coefficients taken from calculations. Other species coefficients estimated from heat capacity, enthalpy, and entropy at 298K.

Species	a_1	a_2	a_3	a_4	a_5	a_6	a_7
SiO_2(g)	7.4037	5.37E-05	-1.09E-08	7.52E-13	0.0	-4.01E+04	-1.63E+01
SiO_2(l)	10.316	-1.92E-9	4.81E-13	-4.58E-17	0.0	-1.15E+05	-5.76E+01
SiO(g) low T	2.3482	4.51E-03	-3.67E-06	1.09E-09	0.0	-1.29E+04	1.10E+01
SiO(g) high T	4.2936	2.08E-04	-6.13E-08	7.14E –12	0.0	-1.38E+04	3.12E-01
Si(g)	1.7553	6.28E-04	-1.30E-07	8.90E-12	0.0	5.42E+04	1.08E+01
$SiCl_3O_2$	1.61E+01	0	0	0	0	-7.58E+04	-4.14E+01
$SiCl_3O_2H$	1.91E+01	0	0	0	0	-9.68E+04	-5.61E+01
$SiCl_3OH$ high T	1.27E+01	3.13E-03	-1.33E-06	2.80E-10	-2.35E-14	-1.05E+05	-3.10E+01
$SiCl_3OH$ low T	4.77E+00	3.86E-02	-6.25E-05	4.79E-08	-1.40E-11	-1.03E+05	6.31E+00
$SiCl_3O$ high T	1.06E+01	2.06E-03	-1.21E-06	3.29E-10	-3.40E-14	-6.64E+04	-2.04E+01
$SiCl_3O$ low T	4.27E+00	2.98E-02	-4.87E+03	3.74E-08	-1.10E-11	-6.52E+04	9.53E+00
$SiCl_2O$ high T	8.25E+00	2.52E-03	-1.49E-06	4.10E-10	-4.28E-14	-5.87E+04	-1.17E+01

Species	a_1	a_2	a_3	a_4	a_5	a_6	a_7
$SiCl_2O$ low T	4.27E+00	1.90E-02	-2.84E-05	2.07E-08	-5.92E-12	-5.79E+04	7.42E+00
SiClO high T	5.72E+00	1.86E-03	-1.12E-06	3.10E-10	-3.27E-14	-2.13E+04	1.00E-01
SiClO low T	3.77E+00	9.20E-03	-1.20E-05	7.80E-09	-2.06E-12	-2.08E+04	9.66E+00
SiClO2H high T	8.76E+00	4.49E-03	-2.16E-06	5.15E-10	-4.87E-14	-8.01E+04	-1.56E+01
SiClO2H low T	2.52E+00	3.08E-02	-4.51E-05	3.24E-08	-9.10E-12	-7.89E+04	1.43E+01
$SiCl_3O_2H$	1.91E+01	0	0	0	0	-9.68E+04	-5.61E+01

4. Results and Analysis

Figure 2 shows typical fluorescence data for five data runs at a distance of 1.2 cm from the burner. These data have been corrected for laser power. The symbols represent the experimental data, and the lines are the LIFBASE simulated spectra (normalized to the data) for the temperatures given by the relative intensities of the experimental $P_1(2)$ and $R_1(14)$ peaks. Below about 900K, the signal-to-noise ratio for the $R_1(14)$ peak is less than one, and although the integrated intensity can still be obtained, the error bars are higher.

Figures 3 and 4 show temperature and OH concentration, respectively, for three basic flame configurations with and without $SiCl_4$: an undiluted stoichiometric H_2/O_2 flame, a stoichiometric H_2/O_2 flame diluted with argon, and an undiluted rich H_2/O_2 flame ($\Phi = 1.2$). The error bars in these figures are likely due mainly to a combination of shot-to-shot instabilities inherent in a Nd:YAG laser and the slight difference in the environment for each shot due to particles.

In general, the flame temperature increased upon addition of $SiCl_4$. This effect was the largest for the stoichiometric undiluted flame, as seen in Figure 3A, where the maximum flame temperature without $SiCl_4$ was 1125K but increased by 180K to 1300K when $SiCl_4$ was added. For the diluted flame (Figure 3B), the temperatures were slightly lower and rose more slowly up to a maximum of 1120K without $SiCl_4$ and 1200K with $SiCl_4$, a temperature rise of 80K. For the rich flame (Figure 3C), the temperature difference upon adding $SiCl_4$ is even less, reaching 1060K for the flame without $SiCl_4$ and only increasing 35K to 1095K for the flame with $SiCl_4$.

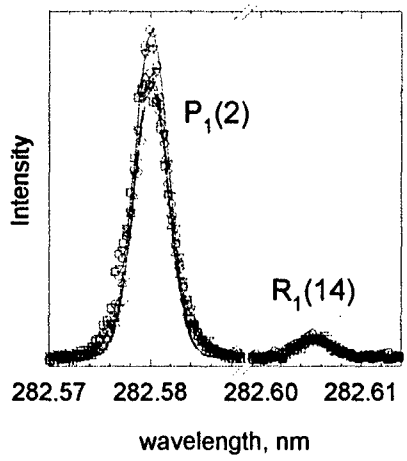

Figure 2. Fluorescence data collected 1.2 cm from the burner for five data runs. The symbols represent the experimental data, and the lines represent the LIFBASE simulated spectrum for the temperature given by the ratio of the areas under the $P_1(2)$ and $R_1(14)$ peaks. The circles and solid line are for run 1 (temperature 1291K), the triangles pointing down and dotted line are for run 2 (temperature 1307K), the squares and short-dashed line are for run 3 (temperature 1253K), the diamonds and dot-dot-dashed line are for run 4 (temperature 1320K), and the triangles pointing up and the long-dashed line are for run 5 (temperature 1260K).

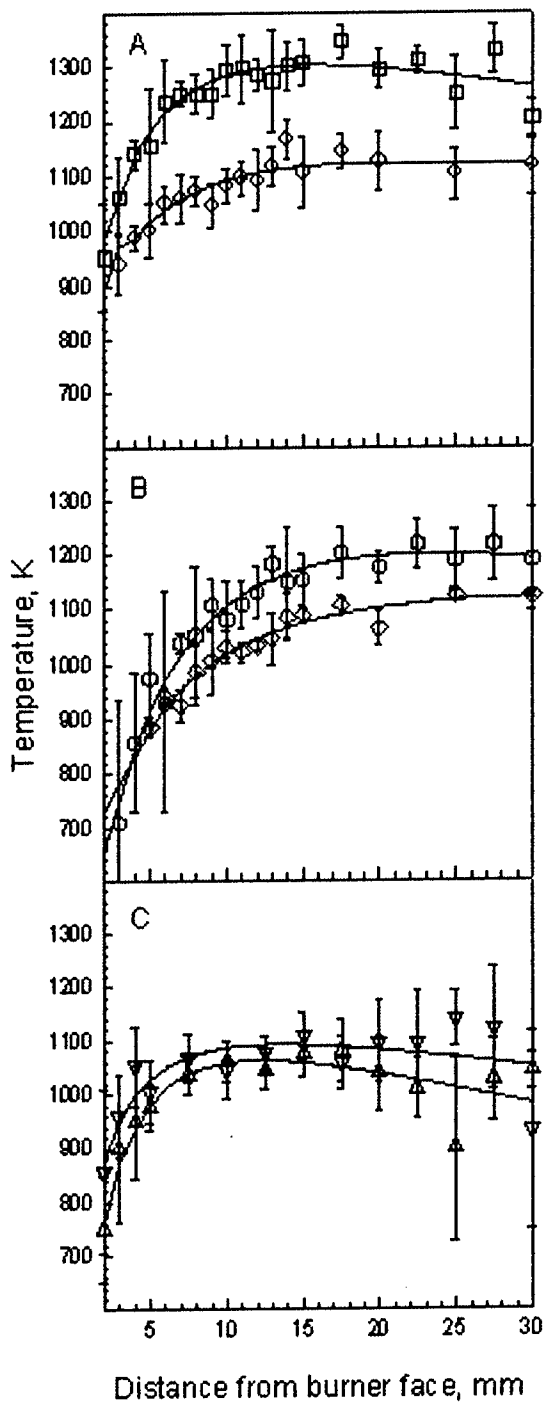

Figure 3. Temperature profiles for hydrogen/oxygen flames with and without $SiCl_4$. (A) shows data for the stoichiometric undiluted flame. The circles indicate data without $SiCl_4$ and the squares show data for the flame with $SiCl_4$. (B) shows data for the stoichiometric diluted flame. The diamonds indicate data without $SiCl_4$ and the hexagons show data for the flame with $SiCl_4$. C) shows data for the rich undiluted flame. The triangles pointing up indicate data without $SiCl_4$ and the triangles pointing down show data for the flame with $SiCl_4$. The lines indicate fits to the temperature data.

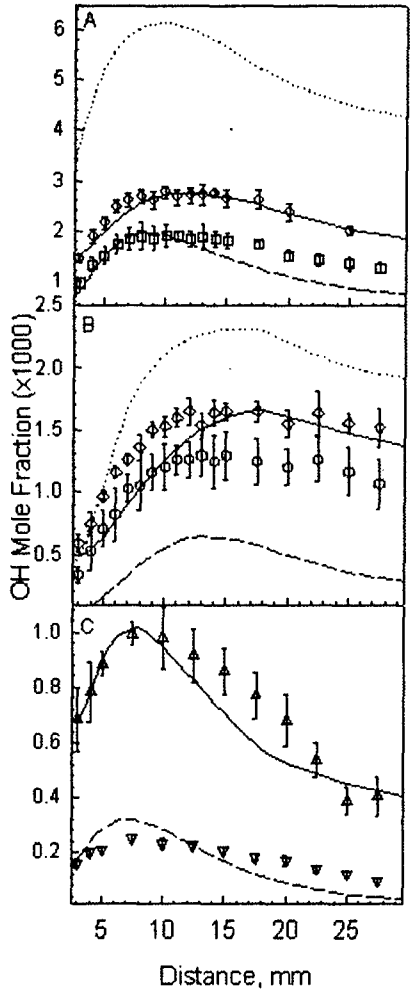

Figure 4. OH concentration profiles for hydrogen/oxygen flames with and without $SiCl_4$. In all panels, the solid lines are the model predictions of OH concentration for the flames without $SiCl_4$, the dashed lines are the model predictions of the OH concentration for the flames with $SiCl_4$ using the modified rates, and the dotted lines are the model predictions of the OH concentration for the flames with $SiCl_4$ using the original rates. A) shows data for the stoichiometric undiluted flame. The circles indicate data without $SiCl_4$ and the squares show data for the flame with $SiCl_4$. B) shows data for the stoichiometric diluted flame. The diamonds indicate data without $SiCl_4$ and the hexagons show data for the flame with $SiCl_4$. C) shows data for the rich undiluted flame. The triangles pointing up indicate data without $SiCl_4$ and the triangles pointing down show data for the flame with $SiCl_4$.

The addition of $SiCl_4$ suppressed the OH concentration for all flame configurations, as can be seen in Figure 4. For the undiluted flame (Figure 4A), the addition of $SiCl_4$ reduced the OH concentration to ~85% of its value without $SiCl_4$. In the diluted flame (Figure 4B), the reduction in OH concentration on addition of $SiCl_4$ was similar, with the $SiCl_4$ flame having ~79% of the OH of the flame without $SiCl_4$. However, in the rich flame (Figure 4C) the reduction was much higher, with the $SiCl_4$ flame having only 35% of the maximum OH observed in the flame without $SiCl_4$. The shape of the OH concentration profile changed more on adding $SiCl_4$ for the rich flame, becoming much more flat than the OH profile without $SiCl_4$.

The model prediction of the OH concentration for the stoichiometric undiluted flame without $SiCl_4$ was within the error bars of the measured values except at 5–7 mm above the burner, where the model slightly underpredicted the OH concentration. The fit to the rich flame without $SiCl_4$ was good for the leading edge and tail of the OH concentration peak, but OH was underpredicted in the region from 15 to 20 mm above the burner. The model prediction of the OH concentration for the diluted flame without $SiCl_4$ significantly underpredicted the OH concentration for the entire leading edge of the OH peak, the region from the burner surface to 12 mm above the burner. Even adjusting the input temperature profile to the extremes of the error bars did not correct this problem. All three of these H_2/O_2 flames without $SiCl_4$ were modeled using the GRI 3.0 mechanism and the premixed burner input to CHEMKIN, so the comparison of the prediction to the experimental data gives some idea of the limitations of this model.

The model prediction of OH concentration for the stoichiometric hot flame with $SiCl_4$ fits well in the leading edge and peak of the OH concentration, but underpredicts the OH in the tail, the region more than 14 mm from the burner. For the rich flame without precursor, the shape of the predicted OH profile is somewhat off, overpredicting OH in the early part of the flame from 4 to 10 mm from the burner and underpredicting in the tail (beyond 15 mm). The experimental OH profile is more flat than the model prediction. However, the magnitude of the OH concentration is correctly predicted. The model significantly underpredicts the OH concentration throughout the entire region for the diluted flame with precursor.

5. Discussion

5.1 Reaction Rates

The initial set of rates chosen for our investigation of the $SiCl_4$ mechanism did not provide a satisfactory fit to the data for any of the flame configurations studied, as can be seen by the dotted lines in Figure 4. It overpredicted the OH concentration by a factor of 3 for the undiluted stoichiometric flame (Figure 4A), a factor of 2 for the diluted flame (Figure 4B), and a factor of 4.5 for the rich flame (Figure 4C). We performed a sensitivity analysis in CHEMKIN to determine which rates affected the OH profile the most. The sensitivities of the OH concentration to various rates for the final rate set are shown in Table 4. While several different combinations of rates could yield a reasonable prediction of the OH concentration for the stoichiometric undiluted flame, we chose the combination that also did the best job at fitting the data from the other two flame configurations. The predicted OH concentration was sensitive to several reactions that do not have well-known rates. Table 5 lists these reactions and the modifications we made to the rate expressions.

Table 4. CHEMKIN Sensitivities of OH Concentration to the Reaction Rates at Different Distances from the Burner. The sensitivities are listed as follows: the undiluted stoichiometric flame in bold, the diluted stoichiometric flame in plain text, and the undiluted rich flame in italics.

Reaction	Distance from burner (cm)			
	0.5	1.0	2.0	3.0
OH + H2 = H + H2O	**-0.797**	**-0.520**	**-0.328**	**-0.288**
	-0.940	-0.844	-0.706	-0.695
	-0.948	*-0.944*	*-0.959*	*-0.957*
H + O2 = O + OH	**0.349**	**0.115**	**-0.079**	**-0.080**
	0.135	0.262	0.046	-0.037
	0.151	*0.034*	*-0.134*	*-0.175*
Cl + H2 = HCl + H	**0.060**	**0.014**	**0.008**	**0.012**
	-0.087	0.043	0.000	-0.004
	0.045	*0.006*	*-0.015*	*-0.022*
2OH = O + H2O	**-0.018**	**-0.035**	**-0.051**	**-0.056**
	-0.009	-0.013	-0.018	-0.015
	-0.002	*-0.001*	*0.000*	*0.001*
H + HO2 = 2OH	**0.010**	**0.000**	**-0.002**	**-0.002**
	0.031	0.006	0.000	-0.002
	0.012	*-0.001*	*-0.011*	*-0.014*
SiO + O2 = SiO2 + O	**0.484**	**0.260**	**0.046**	**-0.102**
	0.698	0.596	0.469	0.375
	0.672	*0.316*	*-0.478*	*-1.325*
SiClO + M = SiO + Cl + M	**-0.230**	**-0.130**	**0.016**	**0.033**
	-0.291	-0.198	-0.072	-0.010
	-0.168	*-0.041*	*0.132*	*0.214*
SiClO + H = SiO + HCl	**-0.095**	**-0.114**	**-0.109**	**-0.104**
	-0.172	-0.092	-0.108	-0.114
	-0.121	*-0.045*	*0.069*	*0.173*

Reaction	Distance from burner (cm)			
	0.5	1.0	2.0	3.0
SiCl4 + H = SiCl3 + HCl	**-0.014**	**-0.024**	**-0.005**	**-0.012**
	0.014	0.019	0.012	0.017
	0.091	*0.039*	*-0.063*	*-0.184*
SiO + OH = SiO2 + H	**0.005**	**0.008**	**0.016**	**0.000**
	0.347	0.009	0.012	0.012
	0.078	*-0.017*	*-0.078*	*-0.139*
SiCl2O + H = SiClO + HCl	**0.007**	**0.000**	**0.000**	**-0.009**
	0.036	0.018	0.024	0.028
	0.029	*0.015*	*-0.016*	*-0.068*
SiCl3 + H = SiCl2 + HCl	**-0.003**	**-0.013**	**-0.004**	**-0.008**
	0.006	0.012	0.008	0.009
	0.022	*0.011*	*-0.018*	*-0.048*
SiCl2O + H2O = SiClO2H + HCl	**-0.004**	**-0.001**	**-0.001**	**0.007**
	-0.013	-0.010	-0.016	-0.019
	-0.016	*-0.013*	*0.006*	*0.048*
SiCl2O + OH = SiClO2H + Cl	**-0.003**	**0.000**	**0.000**	**0.003**
	-0.012	-0.007	-0.008	-0.009
	-0.007	*-0.003*	*0.004*	*0.015*

Table 5. Reactions modified in order to improve the model fit to our data

Reaction	Source	Modification
$SiO + O_2 = SiO_2 + O$	Estimated by Jachimowski[41]	Decrease A by ~ order of magnitude Decrease Ea from 27 to 21 kJ/mol
SiClO + H = SiO + HCl	Estimated by analogy with SiH_4 [5]	Increase A by factor of 150 Ea was estimated to be 0; unchanged
$SiO + OH = SiO_2 + H$	Calculated by Zachariah[3]	Increase A by ~ factor of 2 Decrease Ea from 5 to 0 kJ/mol
SiClO + M = SiO + Cl	Estimated by analogy with SiH_4 [5]	Increase A by factor of 2 Decrease Ea from 121 to 33 kJ/mol
$SiCl4 + H = SiCl_3 + HCl$	Shock tube experiment by Catoire *et al.* [34]	Increase A by ~ 25% Decrease Ea from 40 to 29 kJ/mol
$SiCl_2O + H = SiClO + HCl$	Estimated by analogy with SiH_4 [5]	Increase A by ~ order of magnitude Decrease Ea from 44 to 21 kJ/mol

The rate for the reaction to which the predicted OH concentration profile was most sensitive, SiO + O_2, was thought to be too high by Babushok *et al.*, who estimated an activation energy (E_a) of 125 kJ/mol and an Arrhenius parameter (A) of 5×10^{12} cc/molecule-s. When we used these parameters and adjusted the other reaction parameters until the predicted peak had the observed magnitude for the stoichiometric undiluted flame, the OH concentration was significantly underpredicted in the rising edge and in the tail. The predictions for the other two flame configurations were also poor. The original estimate of $E_a = 27$ kJ/mol and $A = 1 \times 10^{13}$ cc/molecule-s was made by Jachimowski, who used Hirschfelder's rule to estimate the activation energy and analogy to CO to determine the A factor. We reduced the activation energy and the Arrhenius parameter from Jachimowski's estimate to fit our data.

Of the six reactions that we modified to fit our data, one has been experimentally measured. Catoire *et al.*[35] measured the reaction rate of $SiCl_4$ + H in a shock tube experiment at 1530 and 1730K and obtained an Arrhenius parameter of $A = 1.4 \times 10^{13}$ (±24%) cc/molecule-s and an activation energy of

E_a = 40±22 kJ/mol. Our values for the activation energy and Arrhenius parameter fall within the reported experimental error bar range. This rate was also calculated by Zhang *et al.*,[50] who calculated $A = 6.6 \times 10^{14}$ cc/molecule-s and E_a = 113 kJ/mol for the temperature range 1500–1800K. The rate calculated by Zhang is within the error of the experimental measurement over the temperature range in which the measurements were made. Some reasons for the large difference in activation energy between the experiment and the calculation are discussed in Zhang's paper[50] Another consideration is that the basis set used in the calculations, QCISD, has been found to give higher reaction energies and barrier heights than other basis sets for reaction of chlorine with methane.[51] The value for this rate that we used in our model in order to provide the best fit to our data is closer to the experi-mental rate than to the calculated one.

5.2 Temperature

Addition of $SiCl_4$ precursor caused the flame temperature to increase for all three basic flame configurations. An equilibrium analysis based on our model indicates that there is very little energy in the combustion of $SiCl_4$ compared to H_2 and O_2. In fact, combining with H_2 and O_2 to form HCl and SiO_2(g) releases significantly less heat than if the H_2 and O_2 reacted to form H_2O. The only significant heat release comes from the condensation of the silicon oxides; this brings the total heat release up to about the same amount as for water formation. The heat release from particle formation is noticeable because it occurs in a portion of the flame different from the heat release from water formation. Therefore, the region of the flame where the temperature increase is observed could indicate the region of particle formation. $SiCl_4$ has a higher heat capacity than the diatomics H_2 and O_2; this causes a slower rise in temperature in the early portion of the $SiCl_4$-doped flame.

A flame temperature rise upon precursor addition was also observed by Hwang *et al.*[7] as well as by Wilcox *et al.*[52] Hwang *et al.* attributed the increase of ~100K in the region 35 to 80 mm above the burner to heat released during exothermic reactions of $SiCl_4$ oxidation and hydrolysis. Wilcox *et al.* studied a chromium oxide producing premixed low-pressure flame and observed an increase of ~180K 1 cm above the burner upon addition of chromium precursor. They attribute this increase to a shift in the radical concentrations towards equilibrium by heterogeneous radical recombination catalysis on chromium particles. Lehtinen and Zachariah[53] predict that under certain conditions, particle coalescence will result in a heat release to the surrounding gas.

The temperature increase was the largest for the stoichiometric undiluted flame and the smallest for the rich flame. The temperature increase for the diluted flame was a little less than half that of the undiluted flame, which is consistent with the absolute $SiCl_4$ concentration being reduced by a factor of ~0.4 in the diluted flame. For the rich flame, the absolute temperatures are lower, and the temperature difference upon $SiCl_4$ addition is relatively small. The lower temperature reduces the rate of $SiCl_4$ reactions, which delays particle formation. At 3 cm from the burner, 4% of the initial $SiCl_4$ remains in the rich flame, as opposed to <1% for the stoichiometric flames.

5.3 OH concentration

Addition of $SiCl_4$ precursor depleted the OH concentration relative to the flames without precursor for all three basic flame configurations. The rich flame had by far the most depletion on addition of precursor, perhaps because the lower temperatures prolong the processing of $SiCl_4$. The model pre-

diction for the rich flame matches reasonably well in magnitude but not in shape. The model prediction for the diluted flame is very poor, with the model predicting much less OH than is observed. We did attempt to take into account the differences in efficiencies of argon and water as a third body, which did increase the predicted OH a little but not nearly enough. The premixed burner reactor in the CHEMKIN software does not have any provisions for including condensation or surface chemistry, which could affect the OH concentration profile, especially in the tail of the distribution where we expect more particle formation to be occurring.

Zachariah and Burgess[9] measured OH concentration in an atmospheric pressure counter-flow diffusion flame doped with silane and observed an order of magnitude depletion in the OH concentration with respect to the undoped flame. They only observed this depletion in the regions where the precursor was undergoing pyrolysis and particle formation, but not in the particle-laden zone after particle formation was complete. They suggested that OH plays a significant role in the oxidation of Si-containing species and clusters, but doesn't react on the highly hydroxylated particles. Hwang *et al.*[7] measured the OH concentration in an atmospheric pressure co-flow diffusion flame doped with $SiCl_4$, and observed an order of magnitude reduction upon addition of precursor in the particle formation zone but not in other parts of the flame (measured on the centerline). They attributed the OH decrease to equilibrium shifts in the OH concentration caused by consumption of O_2 and H_2O by reaction with $SiCl_4$ as well as OH consumption by reaction with HCl. We observed suppression of OH over our entire measurement range. We did not observe the OH concentration profile with $SiCl_4$ approach its value without $SiCl_4$; however, at low pressure, the particle formation zone is significantly stretched compared to the atmospheric pressure flames such as those in the experiments described above, and all of our measurements fall within the particle formation zone. The model, which does not take particle formation into account, underpredicts OH in the tail of both the undiluted stoichiometric and the rich flames, perhaps suggesting that the particle formation zone is beginning to tail off.

6. Conclusion

Hydroxyl concentration and temperature profiles for $SiCl_4$ combustion in a low-pressure premixed flat flame have been obtained using LIF. These data are sensitive to the overall chemical kinetics of our proposed $SiCl_4$ combustion mechanism. In order to obtain the best fit to the observed data at all three flame configurations, we had to modify six different rates from our original estimates. None of the modified rates are well known in the temperature regime of our flame. Experimental study of these rates in the temperature range from 500K to 1500K would allow us to refine our $SiCl_4$ combustion mechanism. Our model did not predict the correct OH profiles for all conditions. In particular, we had the most trouble fitting the data from the diluted flame, even though the maximum temperatures were similar to those in the undiluted stoichiometric flame, indicating that our mechanism for $SiCl_4$ combustion is not complete. Addition of condensation and heterogeneous chemistry might improve our understanding of this problem. While we did not study the effects of $SiCl_4$ kinetics on final particle characteristics, we found that even in a premixed flame, addition of $SiCl_4$ dopant did affect the temperature and OH concentration profile in the flame. These profiles are determined by the precursor kinetics. Particle formation is very sensitive to temperature history, so precursor kinetics could affect the final particle characteristics. The OH concentration was also found to be sensitive to the flame stoichiometry and diluent.

References

1. M. S. Wooldridge, *Progress in Energy and Combustion Science* **24** (1998) 63.
2. S. E. Pratsinis, *Progress in Energy and Combustion Science* **24** (1998) 197.
3. M. R. Zachariah and W. Tsang, *Journal of Physical Chemistry* **99** (1995) 5308.
4. D. Lindackers, M. G. D. Strecker, P. Roth, C. Janzen, and S. E. Pratsinis, *Combustion Science and Technology* **123** (1997) 287.
5. T. Takahashi, K. E. Hagiwara, and H. Komiyama, *Journal of the Electrochemical Society* **143** (1996) 1355.
6. S. H. Ehrman, S. K. Friedlander, and M. R. Zachariah, *Journal of Aerosol Science* **29** (1998) 687.
7. J. Y. Hwang, Y. S. Gil, J. I. Kim, M. Choi, and S. H. Chung, *Journal of Aerosol Science* **32** (2001) 601.
8. M. D. Allendorf, J. R. Bautista, and E. Potkay, *Journal of Applied Physics* **66** (1989) 5046.
9. M. R. Zachariah and D. F. R. Jr. Burgess, *Journal of Aerosol Science* **25** (1994) 487.
10. H. Briesen, A. Fuhrmann, and S. E. Pratsinis, *Chemical Engineering Science* **53** (1998) 4105.
11. B. Hannebauer and F. Menzel, *Z. Anorg. Allg. Chem.* **629** (2003) 1485.
12. B. W. Lee, S. Oh, and M. Choi, *Aerosol Science and Technology* **35** (2001) 978.
13. A. Tezaki, M. Kazuyo, and H. Matsui, *Journal of Physical Chemistry* **98** (1994) 10529.
14. D. R. Powers, *Journal of the American Ceramic Society* **61** (1978) 295.
15. M. K. Akhtar, S. E. Pratsinis, and S. V. R. Mastrangelo, *Journal of Materials Research* **9** (1994) 1241.
16. D. K. Pal, M. K. Kowar, A. N. Daw, and P. Roy, *Microelectronics Journal* **26** (1995) 507.
17. N. Mayo, U. Carmi, I. Rosenthal, R. Avni, R. Manory, and A. Grill, *Journal of Applied Physics* **55** (1984) 4404.
18. K.-S. Kim, *AIChE Journal - Ceramics Processing* **43** (1997) 2679.
19. D. L. Wood, J. B. Macchesney, and J. P. Luongo, *Journal of Materials Science* **13** (1978) 1761.

20. M. Binnewiess, M. Jerzembeck, and A. Kornick, *Angewandte Chemie,* International Edition in English **30** (1991) 745.

21. K. Jug and D. Wichmann, *Journal of Molecular Structure (Theochem)* **313** (1994) 155.

22. K. Jug and D. Wichmann, *Journal of Molecular Structure (Theochem)* **398-399** (1997) 365.

23. M. E. Coltrin, R. J. Kee, and F. M. Rupley, Sandia Report SAND90-8003B UC-401, (1991).

24. R. J. Kee, R. M. Rupley, J. A. Miller, M. E. Coltrin, J. F. Grcar, E. Meeks, H. K. Moffat, A. E. Lutz, G. Dixon-Lewis, M. D. Smooke, J. Warnatz, G. H. Evans, R. S. Larson, R. E. Mitchell, L. R. Petzold, W. C. Reynolds, M. Caracotsios, W. E. Stewart, P. Glarborg, C. Wang, and O. Adigun, *CHEMKIN Collection* version 3.6, Reaction Design Inc., San Diego, CA, 2000.

25. B. B. Brady and L. R. Martin, *Journal of Spacecraft and Rockets* **34** (1997) 780.

26. B. B. Brady and L. R. Martin, *Atmospheric Environment* **29** (1995) 715.

27. B. Brady, L. R. Martin, and V. I. Lang, *Journal of Spacecraft and Rockets* **34** (1997) 780.

28. A. McIlroy and L. K. Johnson, *Combustion Science and Technology* **116** (1996) 31.

29. J. W. Daily, *Progress in Energy Combustion Science* **23** (1997) 133.

30. A. Lawitzki, I. Plath, W. Stricker, J. Bittner, U. Meier, and K. Kohse-Höinghaus, *Applied Physics* B **50** (1990) 513.

31. U. Meier, R. Kienle, I. Plath, and K. Kohse-Höinghaus, *Ber. Busenges. Phys. Chem.* **96** (1992) 1401.

32. J. Luque and D. R. Crosley, SRI International Report MP-99-009, (1999).

33. R. D. Kenner, F. Rohrer, and F. Stuhl, *Journal of Physical Chemistry* **93** (1989) 7824.

34. L. Catoire, D. Woiki, and P. Roth, *International Journal of Chemical Kinetics* **29** (1997) 415.

35. L. Catoire, D. Woiki, and P. Roth, *International Journal of Chemical Kinetics* **29** (1997) 469.

36. J. T. Niiranen and D. Gutman, *J. Phys. Chem.* **97** (1993) 4106.

37. V. Sandhu, A. Jodhan, I. Safarik, O. P. Strausz, and T. N. Bell, *Chemical Physics Letters* **135** (1987) 260.

38. S. Nitodas and S. V. Sotirchos, *Journal of the Electrochemical Society* **149** (2002) C112-C119.

39. M. D. Allendorf and T. H. Osterheld, *Mat. Res. Soc. Symp. Proc.* **363** (1995) 39.

40. V. F. Kochubei, *Kinetics and Catalysis* **38** (1997) 212.

41. C. J. Jachimowski and A. G. McLain,NASA Technical Paper 2129.

42. V. I. Babushok, W. Tsang, D. R. Jr. Burgess, and M. R. Zachariah, Twenty-Seventh Symposium (International) on Combustion, Pittsburgh, (The Combustion Institute, 1998), p. 2431.

43. National Institute of Standards and Technology, Web Page, *NIST Webbook* (Available: http://webbook.nist.gov, December 2001).

44. G. P. Smith *et al.*, Web Page, *GRI-Mech 3.0* (Available: http://www.me.berkeley.edu/gri_mech/, 2002).

45. R. C. Reid, J. M. Prausnitz, and T. K. Sherwood, *The Properties of Gases and Liquids*, Third Edition ed. (McGraw-Hill Book Company, New York, 1977).

46. D. R. Lide, *CRC Handbook of Chemistry and Physics*, 77th ed. (CRC Press, 1997, Boca Raton).

47. M. J. Frisch, G. W. Trucks, H. B. Schlegel, G. E. Scuseria, M. A. Robb, J. R. Cheeseman, V. G. Zakrzewski, J. A. Jr. Montgomery, R. E. Stratmann, J. C. Burant, S. Dapprich, J. M. Millam, A. D. Daniels, K. N. Kudin, M. C. Strain, O. Farkas, J. Tomasi, V. Barone, M. Cossi, R. Cammi, B. Mennucci, C. Pomelli, C. Adamo, S. Clifford, J. Ochterski, G. A. Petersson, P. Y. Ayala, Q. Cui, K. Morokuma, D. K. Malick, A. D. Rabuck, K. Raghavachari, J. B. Foresman, J. Cioslowski, J. V. Ortiz, A. G. Baboul, B. B. Stefanov, G. Liu, A. Liashenko, P. Piskorz, I. Komaromi, R. Gomperts, R. L. Martin, D. J. Fox, T. Keith, M. A. Al-Laham, C. Y. Peng, A. Nanayakkara, C. Gonzalez, M. Challacombe, P. M. W. Gill, B. G. Johnson, W. Chen, M. W. Wong, J. L. Andres, M. Head-Gordon, ReplogleE. S. , and J. A. Pople, *Gaussian 98* version Revision A.9, Gaussian, Inc., Pittsburgh PA, 1998.

48. M. W. Chase and et al., *JANAF Thermochemical Tables, Third Edition* ed. (American Chemical Society , 1985).

49. M. D. Allendorf, C. F. Melius, P. Ho, and M. R. Zachariah, *Journal of Physical Chemistry* **99** (1995) 15285.

50. X. Zhang, Y. Ding, Z. Li, X. Huang, and C. Sun, *Phys. Chem. Chem. Phys.* **3** (2001) 965.

51. W. T. Duncan and T. N. Truong, *Journal of Chemical Physics* **103** (1995) 9642.

52. B. P. Wilcox, A. McIlroy, E. t. H. Chrysostom, J. W. Daily, and I. M. Kennedy, *Proceedings of the Western States Combustion Meeting,* UC San Diego, (2002).

53. K. E. J. Lehtinen and M. R. Zachariah, *Journal of Aerosol Science* **33** (2002) 357.

This report reprinted by permission of Elsevier from "Measurements and Modeling of $SiCl_4$ Combustion ina Low-Pressure H_2/O_2 Flame," by T,. Moore, B. Brady, and L. R. Martin, *Combustion & Flame*, **146**, 407–418, 2006 by The Combustion Institute.

LABORATORY OPERATIONS

The Aerospace Corporation functions as an "architect-engineer" for national security programs, specializing in advanced military space systems. The Corporation's Laboratory Operations supports the effective and timely development and operation of national security systems through scientific research and the application of advanced technology. Vital to the success of the Corporation is the technical staff's wide-ranging expertise and its ability to stay abreast of new technological developments and program support issues associated with rapidly evolving space systems. Contributing capabilities are provided by these individual organizations:

Electronics and Photonics Laboratory: Microelectronics, VLSI reliability, failure analysis, solid-state device physics, compound semiconductors, radiation effects, infrared and CCD detector devices, data storage and display technologies; lasers and electro-optics, solid-state laser design, micro-optics, optical communications, and fiber-optic sensors; atomic frequency standards, applied laser spectroscopy, laser chemistry, atmospheric propagation and beam control, LIDAR/LADAR remote sensing; solar cell and array testing and evaluation, battery electrochemistry, battery testing and evaluation.

Space Materials Laboratory: Evaluation and characterizations of new materials and processing techniques: metals, alloys, ceramics, polymers, thin films, and composites; development of advanced deposition processes; nondestructive evaluation, component failure analysis and reliability; structural mechanics, fracture mechanics, and stress corrosion; analysis and evaluation of materials at cryogenic and elevated temperatures; launch vehicle fluid mechanics, heat transfer and flight dynamics; aerothermodynamics; chemical and electric propulsion; environmental chemistry; combustion processes; space environment effects on materials, hardening and vulnerability assessment; contamination, thermal and structural control; lubrication and surface phenomena. Microelectromechanical systems (MEMS) for space applications; laser micromachining; laser-surface physical and chemical interactions; micropropulsion; micro- and nanosatellite mission analysis; intelligent microinstruments for monitoring space and launch system environments.

Space Science Applications Laboratory: Magnetospheric, auroral and cosmic-ray physics, wave-particle interactions, magnetospheric plasma waves; atmospheric and ionospheric physics, density and composition of the upper atmosphere, remote sensing using atmospheric radiation; solar physics, infrared astronomy, infrared signature analysis; infrared surveillance, imaging and remote sensing; multispectral and hyperspectral sensor development; data analysis and algorithm development; applications of multispectral and hyperspectral imagery to defense, civil space, commercial, and environmental missions; effects of solar activity, magnetic storms and nuclear explosions on the Earth's atmosphere, ionosphere and magnetosphere; effects of electromagnetic and particulate radiations on space systems; space instrumentation, design, fabrication and test; environmental chemistry, trace detection; atmospheric chemical reactions, atmospheric optics, light scattering, state-specific chemical reactions, and radiative signatures of missile plumes.